Accurate Extrinsic and Intrinsic peak broadening modeling for time-resolved in situ ball milling reactions via synchrotron powder X-ray diffraction

Paolo P. Mazzeo,*[a,b] Giulio I. Lampronti,*[c] Adam L. Michalchuk,[d] Ana M. Belenguer,[e] Alessia Bacchi,[a,b] and Franziska Emmerling [c]

[a] *Department of Chemistry, Life Sciences and Environmental Sustainability, University of Parma, Parco Area delle Scienze 17/A, 43124 Parma, Italy.*
[b] *Biopharmanet-TEC, University of Parma, Parco Area delle Scienze 27/A, 43124 Parma, Italy*
[c] *Department of Materials Science & Metallurgy, Univesrity of Cambridge, 27 Charles Babbage Rd, Cambridge CB3 0FS*
[d] *BAM Federal Institute for Materials Research and Testing, Richard-Willstätter-Straße 11, D-12489 Berlin, Germany.*
[e] *Yusuf Hamied Department of Chemistry, University of Cambridge, Lensfield Road, Cambridge CB2 1EW, UK.*

Supporting information

Ball mill grinder 2
Milling Jar Design 2
X-ray transmission of Perspex (PMMA) 2
Milling jar specs 3
Si640d standard Jar alignment 4
Quantitative Phase Analyses and microstructural evolution analysis details 6
Peak shape definition 7
Instrumental Resolution function (IRF) 8
TCHZ function output parameters 9
Rietveld refinement of ex-situ data 11
Microstrain parameter definition 12
Details of neat grinding reactions 13
Inorganic metathesis reaction by neat grinding 13
Synthesis of Theophylline:Benzamide cocrystals 15
TOPAS custom Macros 16
Sample displacement macro 16
Sample displacement macro with extra empirical correction 16
TCHZ Peak profile for the split peak 17
Refinement of the peak split 17

Ball mill grinder

The ball mill grinding experiments at BESSY II were all performed using a Fritsch P23 vertical movement Shaker Mill, **Figure SI 1**. This mill has a fixed amplitude of 9 mm and adjustable frequency from 15 Hz to 50 Hz with an adjustable timer. An adaptor was made in house (BAM) to ensure that the milling jar were kept in position during grinding.

Figure SI 1| Fritsch Pulverisette 23 (P23) in its standard configuration with commercial jar included.

Milling Jar Design

All experiments were conducted using a custom design of milling jars prepared at the mechanical workshop at BAM.

X-ray transmission of Perspex (PMMA)

Perspex has been traditionally selected for TRIS mechanochemical investigations owing to its low absorption coefficient for X-rays. Lower energy X-rays are less penetrating through organic phases and hence careful consideration of jar thickness at these energies was critical. Simulated absorption coefficients, **Figure SI 2**, suggest that 0.5 mm Perspex absorbs only *ca.* 5% of incident photons at 17 keV, increasing to *ca.* 10% by 1 mm. At 17 keV, we therefore expect our milling jars (2 x 0.75 mm walls) to absorb *ca.*17% of the incident photons for the small and tiny jars.

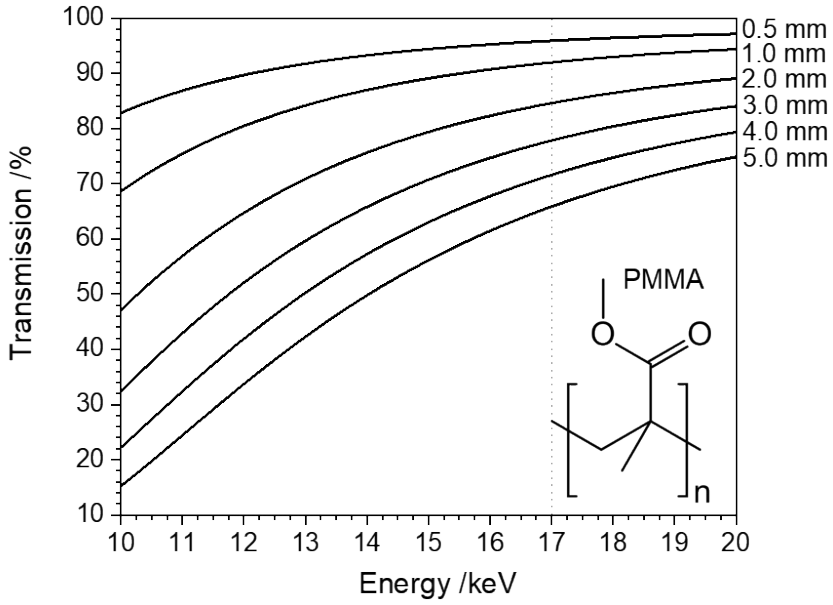

Figure SI 2 | Simulation of X-ray transmission through various thicknesses of Perspex (PMMA, $C_5H_8O_2$, density 1.19 g.cm^{-3}).

Milling jar specs

A 2.3 mL jar is comprised of three pieces, two stainless steel or polyvinyl chloride (PVC) end pieces and a transparent Perspex middle segment of 0.75 mm thickness as shown in **Figure SI 3**. The end pieces were made to have hemispherical internal geometry to allow access of the milling ball to all areas of the internal volume. The overall dimensions of the milling jar are shown in **Figure SI 3b**). The walls of the Perspex piece were 0.75 mm in thickness, and its X-ray diffraction profile is shown in **Figure SI 4.**

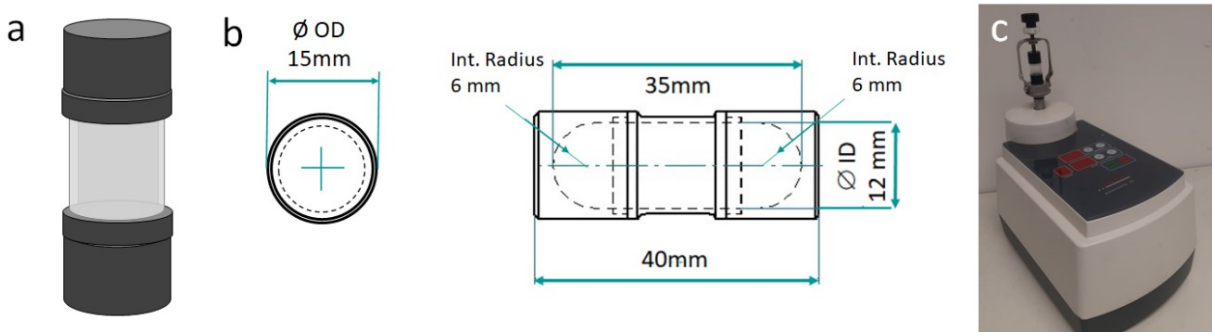

Figure SI 3| Custom built 2.3 mL grinding jar; a) the central Perspex transparent cylindrical part is snap-closed to the top and bottom hemispheric caps made either of stainless steel or polyvinyl chloride; b) mechanical drawing of this jar; c) photograph of the jar installed into the Fritsch P23 vertical vibratory mill.

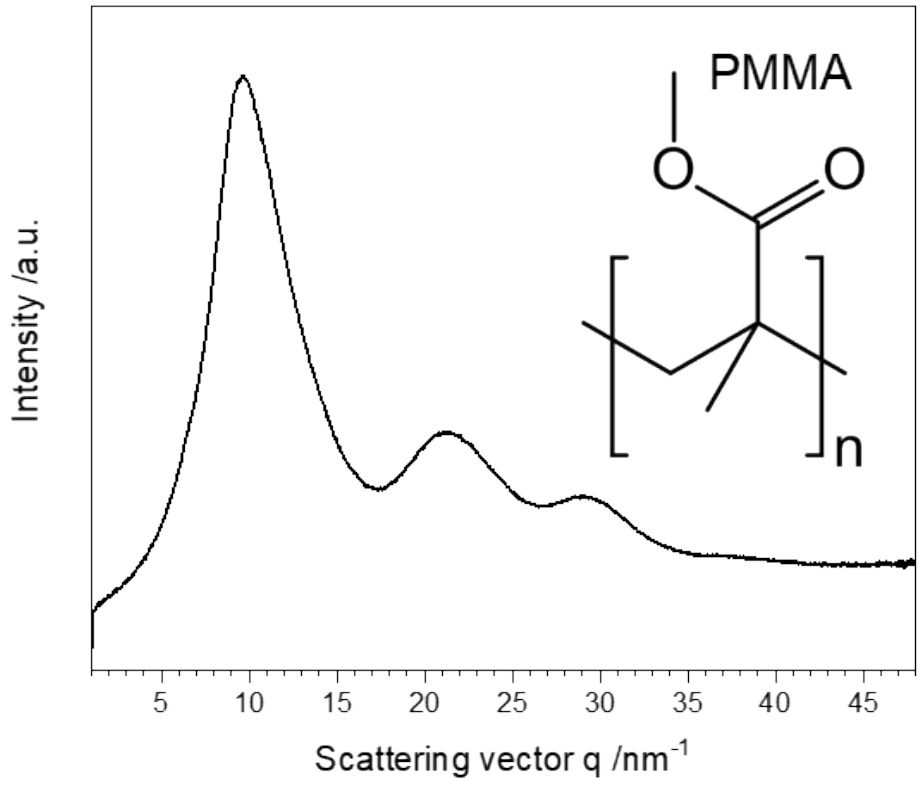

Figure SI 4| Integrated diffraction profile for the empty 2.3 mL small Perspex (PMMA) jar

Si640d standard Jar alignment

Silicon standard was milled for 30 minutes while XRPD data were acquired. Five different TRIS-XRPD experiment were perfomerd with the jar reciprocally aligned in different position with respect to the beam path.
In **Figures SI 5-9** the cascade plots superimposition of XRPD patterns collected for the Si640d as a function of time are reported. Each plot is respresentative of a different alignment position of the jar.

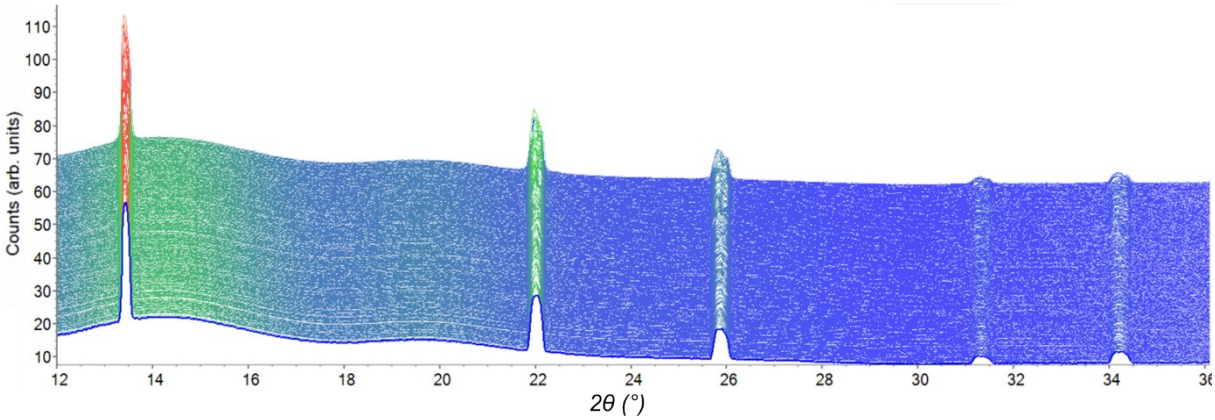

Figure SI 5| Cascade superimposition of TRIS-XRPD data from Si640d collected under milling conditions (one 5mm SS ball bearing, 30 mins, 50 Hz) at the jar position tangential to the beam path. The first and the last patterns are highlighted in blue.

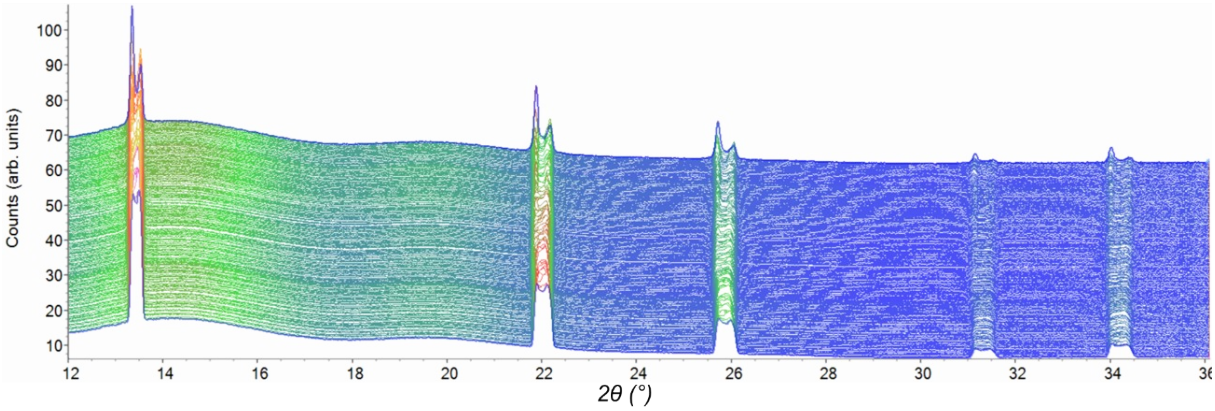

Figure SI 6| Cascade superimposition of TRIS-XRPD data from Si640d collected under milling conditions (one 5mm SS ball bearing, 30 mins, 50 Hz) at the jar position +100µm from the ideal tangential alignment respect to the beam path. The first and the last patterns are highlighted in blue.

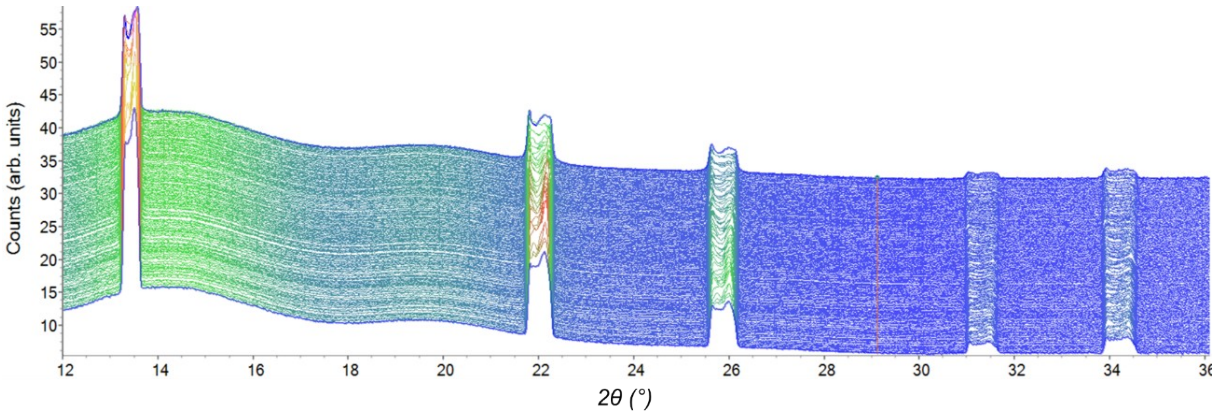

Figure SI 7| Cascade superimposition of TRIS-XRPD data from Si640d collected under milling conditions (one 5mm SS ball bearing, 30 mins, 50 Hz) at the jar position +200µm from the ideal tangential alignment respect to the beam path. The first and the last patterns are highlighted in blue.

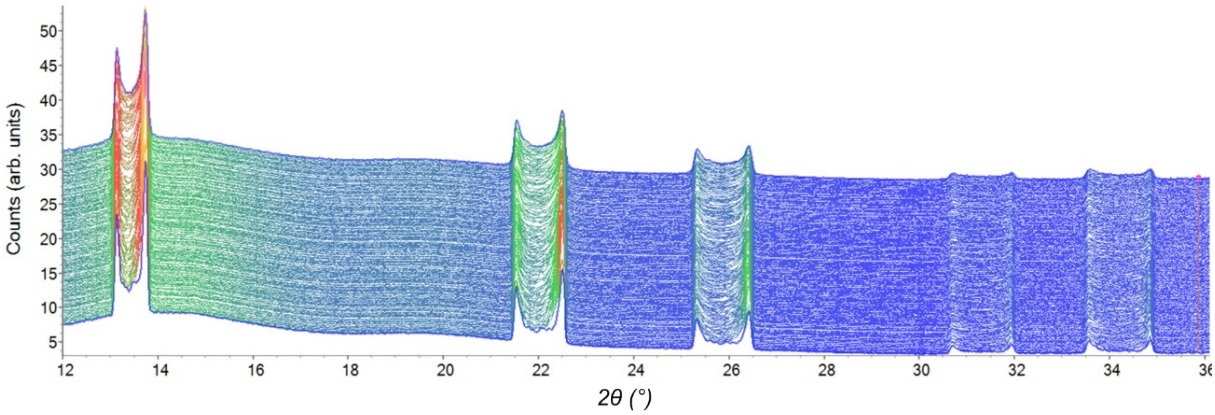

Figure SI 8| Cascade superimposition of TRIS-XRPD data from Si640d collected under milling conditions (one 5mm SS ball bearing, 30 mins, 50 Hz) at the jar position +300µm from the ideal tangential alignment respect to the beam path. The first and the last patterns are highlighted in blue.

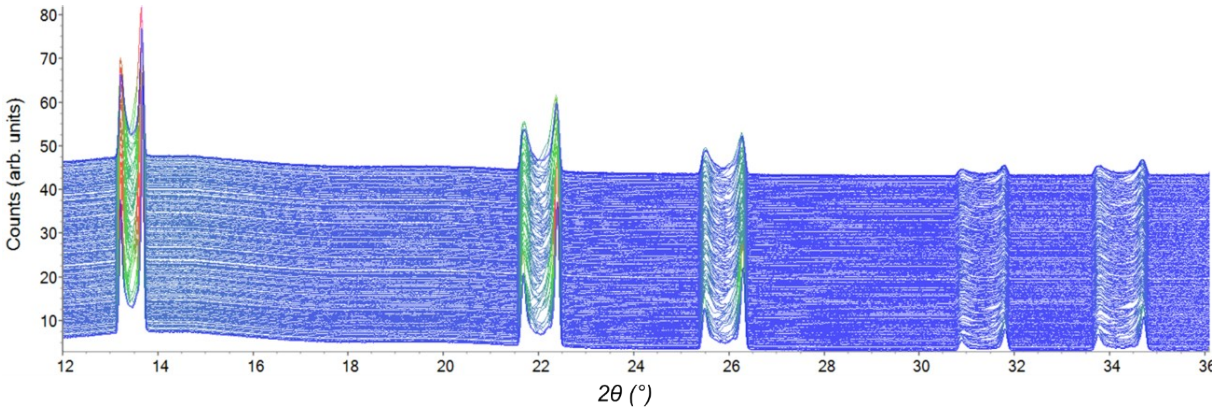

Figure SI 9|. Cascade superimposition of TRIS-XRPD data from Si640d collected under milling conditions (one 5mm SS ball bearing, 30 mins, 50 Hz) at the jar position +400µm from the ideal tangential alignment respect to the beam path. The first and the last patterns are highlighted in blue.

Quantitative Phase Analyses and microstructural evolution analysis details

Rietveld QPA of experimental diffraction patterns was performed using TOPAS-Academic V6. The structural models were retrieved from either the CSD or the ICSD database. XRPD datasets were fit sequentially, with a convergence criterion of 0.0005 and a maximum number of iterations of 1000. An experimental, fixed background profile measured on an empty section of the jar before milling, together with a seventh-order Chebychev polynomial. As described for the Si standard, the crystal structure model of each compound was introduced twice ("top phase" and "bottom phase" from here on) with two distinct TCHZ peak shape functions (with fixed parameters as refined on the Si standard) and independent scale parameters. The composition of the top phase assemblage and that of the bottom phase assemblage were kept equal by setting the scale factor of each bottom phase to be equal to that of the corresponding top phase with a multiplication factor common to all bottom phases. Microstructural investigations were performed assuming that the sample contribution to peak broadening was related to size only. A Lorentzian function was convoluted for each phase, with a single isotropic Crystal Size (CS) parameter related to Γ_L as in the Scherrer equation (**Supplementary Equations 1 and 2**),

$$L(nm) = \frac{K_s \lambda}{(cos\theta) * 10 * \tau}$$ Supplementary Equation 1

$$\Gamma_L = \frac{57.32 * \lambda}{cos\theta * CS}$$ Supplementary Equation 2

in which, L is the mean size of the ordered (crystalline) domains, K_s is a shape factor constant in the range (typically 0.9), λ is the X-ray wavelength, τ is the peak width in radians at FWHM. The top and bottom phases of the same compound were constrained to have the same CS parameter. We here remind that the estimated standard deviation (ESD) from the Rietveld calculation has no bearing on the precision or accuracy, but is merely related to the mathematical fit of the model.

While the visual inspection of a Rietveld plot is the most reliable way to determine the quality of a fit, this is not practical for large datasets, such as those presented here. A global check of a sequential refinement can be efficiently performed by comparing a number of "goodness of fit" indices. One is the weighted profile R-factor (R_{wp}),

$$R_{wp}^2 = \frac{\sum_i w_i (y_{c,i} - y_{o,i})^2}{\sum_i w_i (y_{o,i})^2}$$ Supplementary Equation 3

Where y_c and y_o represent the calculated and observed intensity respectively for each point i. and the weight w_i is equal to $1/\sigma^2[y_{o,i}]$. The second index is "chi squared":

$$\chi^2 = \left(\frac{R_{wp}}{R_{exp}}\right)^2$$ Supplementary Equation 4

where (R_{exp}), the "expected R factor", is:

$$R_{exp}^2 = \frac{N}{\sum_i w_i (y_{o,i})^2}$$ Supplementary Equation 5

with *N* as the number of data points.

Peak shape definition

The dependence of the profile full-width-at-half-max (FWHM) on 2θ was described with a modified Thompson-Cox-Hasting pseudo-Voigt TCHZ function where U, V, W (Gaussian) and X (Lorenzian) are the parameters that have been refined in the current case.

$$TCHZ = \eta\Gamma_L + (1-\eta)\Gamma_G \quad \text{Supplementary Equation 6}$$

$$\Gamma_G = \sqrt{(Utan^2\theta + Vtan\theta + W + Z/cos^2\theta)} \quad \text{Supplementary Equation 7}$$

$$\Gamma_L = \frac{X}{cos\theta} + Ytan\theta \quad \text{Supplementary Equation 8}$$

$$\eta = 1.336603\, q - 0.47719\, q^2 + 0.1116\, q^3 \quad \text{Supplementary Equation 9}$$

$$q = \Gamma_L/\,\Gamma \quad \text{Supplementary Equation 10}$$

$$\Gamma = \sqrt{\Gamma_G^5 + A\Gamma_G^4\Gamma_L + B\Gamma_G^3\Gamma_L^2 + C\Gamma_G^2\Gamma_L^3 + D\Gamma_G\Gamma_L^4 + \Gamma_L^5} = FWHM \quad \text{Supplementary Equation 11}$$

$$A = 2.69269;\ B = 2.42843;\ C = 4.47163;\ D = 0.07842 \quad \text{Supplementary Equation 12}$$

Where η is the Pseudo-Voigt mixing parameter, and Γ_G and Γ_L are the Gaussian and Lorentzian full width half maxima, respectively. Additionally, to model the evident peak asymmetry, the TCHZ was further split to differentiate the contribution at the left-hand side and at the right-hand site to the overall peak profile for the inner and outer scattering vectors $\vec{s_1}$ and $\vec{s_3}$. The final $TCHZ_{split}$ function is applied to describe the overall dependence of the FWHM according to **Supplementary Equation 13** (*vide infra* for macro TCHZ_Split_Peak_Type),

$$TCHZ_{split} = \left(\eta\Gamma_L + (1-\eta)\Gamma_G\right)_{Left} + \left(\eta\Gamma_L + (1-\eta)\Gamma_G\right)_{Right} \quad \text{Supplementary Equation 13}$$

A further Gaussian function was convoluted to empirically describe the dependence of the peak FWHM on the actual size of the jar at the position of the beam. In other words, the FWHM of $\vec{s_2}$ is influenced by the length of the beam path through the jar (see e.g. **Figures 2 and 3** in the main manuscript).

Instrumental Resolution function (IRF)

Rietveld refinement was performed of Si640d TRIS-XRPD pattern collected after 2 mins of milling. The peak split due to the geometrical constrains imposed by out milling setup, mirrors the aberration of the profile full-width-at-half-maximum (FWHM) as a function of 2θ degree, that was described with a modified Thompson-Cox-Hasting pseudo-Voigt TCHZ function. Moreover, to model the evident peak asymmetry, the TCHZ was further split to differentiate the contribution at the left-hand side and at the right-hand site to the overall peak profile for the inner and outer scattering contribution $\vec{s}_1$ and $\vec{s}_3$.
The TCHZ peak function parameters were extracted from a concomitant Rietveld refinement of the five patterns (R_{wp} = 1.72). Alternatively, we refined the TCHZ parameters individually from each XRPD pattern. Although the peak profile changes significantly as function of the jar alignment, our refinement strategy compensates for the sample displacement thus returning almost identical values of TCHZ parameters from any of the patterns collected (**Figure SI 10**).

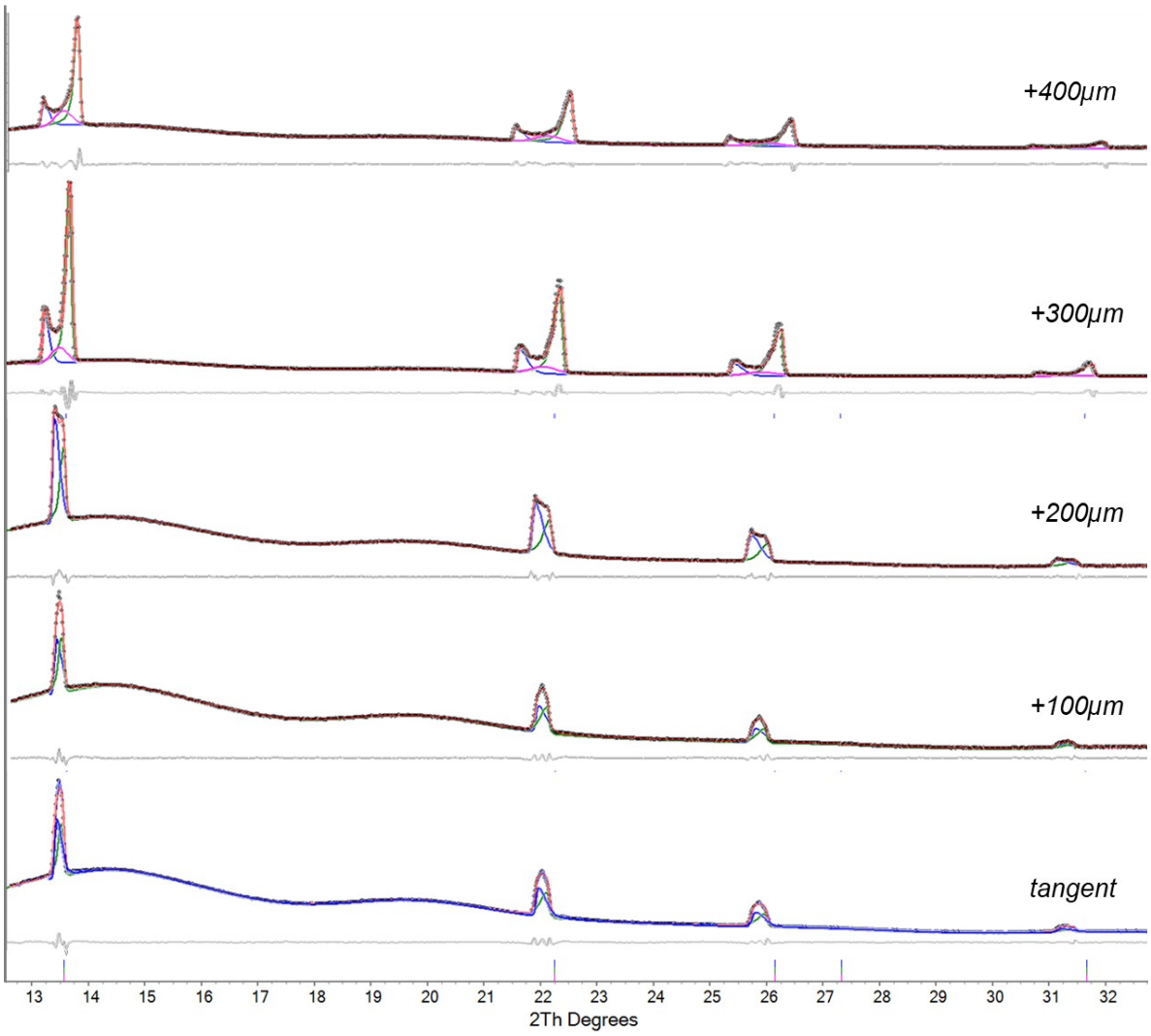

Figure SI 10| Superimposition of Rietveld refinement plot of XRPD pattern collected from the Si640d at different jar positions progressively moved apart from the tangent position with respect to the beam path. Calculated profile (red curve) is plotted against experimental data (black dots). Difference plot Y_{obs}-Y_{calc} is reported in gray. Blue and green curves represent the modelled contribution of the scattering from the powder adhered to the jar wall (namely $\vec{s}_1$ and $\vec{s}_3$). The pink curve represents the modelled contribution of the scattering from the powder randomly disperse within the jar (namely $\vec{s}_2$).

For all Silicon data, particularly when collected with the jar aligned in a general position, we observed a slight mismatch between the modelled curve and the experimental data at higher angular values. This misinterpretation of the angular position is particular evident for patterns characterized by a high sample displacement, namely when the jar is aligned sensibly apart from the beam path.

An empirical correction has been added to the sample displacement function as follow:

$$\Delta 2\theta_{hkl} = \arcsin\left(\left(\frac{\mathbb{d}_L}{R_{DS}}\sin 2\theta_{hkl}\right) + m \cdot \tan^2(2\theta_{hkl})\right) \qquad \text{Supplementary Equation 14}$$

It is worth nothing that this further geometrical misalignment was only detected with sharp silicon peaks, while it has never been observed with real samples, neither for the inorganic metathesis. This further correction is need to mitigate the parallax effect due to the use of large area detectors.

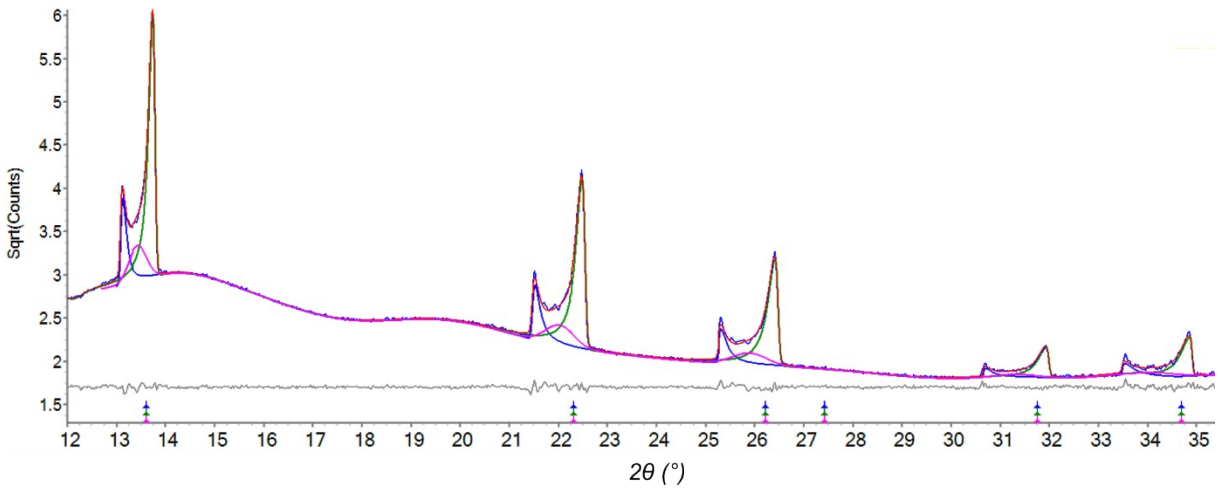

Figure S11. Rietveld plots of the Silicon XRPD patterns collected with the jar aligned 300μm apart from the ideal tangent position to the beam path. Calculated curve (red line) plotted against experimental data (black line). Differential pattern Yobs-Ycal is reported in grey. Rietveld refinement performed applying the empirical correction to the sample displacement; R_{wp}=1.400.The contribution to the overall peak shape of the sample distributed within the jar is highlighted with different colours: the scattering vectors are produced by the sample located at the jar wall closer to the source ($\vec{s_1}$, green line), the wall nearer the detector ($\vec{s_3}$, blue line), and by the sample distributed randomly within the jar ($\vec{s_2}$, pink line).

TCHZ function output parameters

We here report the TOPAS output parameters of the TCHZ function as obtained from Rietveld refinement. It is worth nothing that the contribution of $\vec{s_2}$ become necessary only when the jar is generously moved apart from the beam path position (300 μm from the ideal tangent position).

- Rietveld refinement concomitantly performed over the five XPRD patterns of Si640d standard collected with the jar aligned in different position. Data are reported according to TOPAS formatting code.

```
            TCHZ_Split_Peak_Type(TCHZ01,-0.17763`_0.00095,TCHZ02,
0.06880_0.00415,TCHZ03,-0.00488`_0.00005,,    0,TCHZ04,    0.04083`_0.00599,,
0,TCHZ05,-0.04958`_0.09928,TCHZ06,         0.09417`_0.03434,TCHZ07,         -
0.00259`_0.00269,, 0,TCHZ08, 0.33386`_0.02001,, 0)

            TCHZ_Split_Peak_Type(TCHZ09,-0.31591`_0.02222,TCHZ15,
0.01,TCHZ10,  0.00544`_0.00047,,  0,TCHZ11,  0.42519`_0.01609,,  0,TCHZ12,-
0.11083`_0.00681,TCHZ13,         0.04437`_0.00276,TCHZ14,-0.00185`_0.00021,,
0,TCHZ16, 0.00010`_0.00614,, 0)

            User_Defined_Dependence_Convolution(gauss_fwhm,     (2  Th)     ,
fwhm_middle, 1.30858`_0.03915 min 0.1 max 2)
```

- Rietveld refinement performed on the XRPD pattern of Si640d collected with the jar tangential with respect to the beam path.

```
            TCHZ_Split_Peak_Type(TCHZ01,-0.17674`_0.00383,TCHZ02,
0.06880_0.00415,TCHZ03,-0.00484`_0.00025,,    0,TCHZ04,    0.05983`_0.04006,,
0,TCHZ05,-0.10179`_0.33203,TCHZ06,         0.08731`_0.14143,TCHZ07,         -
0.00315`_0.01203,, 0,TCHZ08, 0.31689`_0.10326,, 0)
```

```
            TCHZ_Split_Peak_Type(TCHZ09,-0.32581`_0.25263,TCHZ15,
0.01,TCHZ10,  0.00542`_0.00519,,  0,TCHZ11,  0.40000`_0.08202,,  0,TCHZ12,-
0.11037`_0.05243,TCHZ13,        0.04450`_0.02233,TCHZ14,-0.00182`_0.00185,,
0,TCHZ16, 0.00010`_0.06916,, 0)
```

- Rietveld refinement performed on the XRPD pattern of Si640d collected with the jar aligned 100µm apart from the tangent position with respect to the beam path.

```
            TCHZ_Split_Peak_Type(TCHZ01,-0.17754`_0.00151,TCHZ02,
0.06880_0.00415,TCHZ03,-0.00496`_0.00008,,   0,TCHZ04,   0.05596`_0.01197,,
0,TCHZ05,-0.05835`_0.20143,TCHZ06,        0.09231`_0.09562,TCHZ07,        -
0.00278`_0.00641,, 0,TCHZ08, 0.32090`_0.05518,, 0)

            TCHZ_Split_Peak_Type(TCHZ09,-0.34670`_0.23263,TCHZ15,
0.01,TCHZ10,  0.00593`_0.00470,,  0,TCHZ11,  0.42752`_0.07246,,  0,TCHZ12,-
0.10635`_0.02891,TCHZ13,        0.04557`_0.01130,TCHZ14,-0.00165`_0.00090,,
0,TCHZ16, 0.00015`_0.03005,, 0)
```

- Rietveld refinement performed on the XRPD pattern of Si640d collected with the jar aligned 200µm apart from the tangent position with respect to the beam path.

```
            TCHZ_Split_Peak_Type(TCHZ01,-0.17849`_0.00458,TCHZ02,
0.06880_0.00415,TCHZ03,-0.00470`_0.00028,,   0,TCHZ04,   0.09580`_0.03803,,
0,TCHZ05,-0.10602`_0.30453,TCHZ06,        0.08844`_0.11660,TCHZ07,        -
0.00314`_0.00994,, 0,TCHZ08, 0.32957`_0.08288,, 0)


            TCHZ_Split_Peak_Type(TCHZ09,-0.33790`_0.22292,TCHZ15,
0.01,TCHZ10,  0.00456`_0.00408,,  0,TCHZ11,  0.31824`_0.08337,,  0,TCHZ12,-
0.12108`_0.05860,TCHZ13,        0.04389`_0.02680,TCHZ14,-0.00161`_0.00222,,
0,TCHZ16, 0.00010`_0.07484,, 0)
```

- Rietveld refinement performed on the XRPD pattern of Si640d collected with the jar aligned 300µm apart from the tangent position with respect to the beam path.

```
            TCHZ_Split_Peak_Type(TCHZ01,-0.18207`_0.00175,TCHZ02,
0.06880_0.00415,TCHZ03,-0.00460`_0.00012,,   0,TCHZ04,   0.00010`_0.01305,,
0,TCHZ05,                 0.09016`_0.16186,TCHZ06,-0.05018`_0.05054,TCHZ07,
0.00708`_0.00393,, 0,TCHZ08, 0.61414`_0.08563,, 0)

            TCHZ_Split_Peak_Type(TCHZ09,-0.18928`_0.02270,TCHZ15,
0.01,TCHZ10,-0.00135`_0.00018,,  0,TCHZ11,  0.49338`_0.03023,,  0,TCHZ12,-
0.12360`_0.00970,TCHZ13,        0.04479`_0.00379,TCHZ14,-0.00218`_0.00029,,
0,TCHZ16, 0.04057`_0.00735,, 0)

            User_Defined_Dependence_Convolution(gauss_fwhm,     (2  Th)     ,
fwhm_middle, 1.63372`_0.07125 min 0.1 max 2)
```

- Rietveld refinement performed on the XRPD pattern of Si640d collected with the jar aligned 400µm apart from the tangent position with respect to the beam path.

```
            TCHZ_Split_Peak_Type(TCHZ01,-0.17989`_0.00131,TCHZ02,
0.06880_0.00415,TCHZ03,-0.00463`_0.00010,,    0,TCHZ04,    0.00010`_0.00940,,
0,TCHZ05,      0.12725`_0.21232,TCHZ06,      0.09608`_0.06932,TCHZ07,      -
0.00539`_0.00537,, 0,TCHZ08, 0.34888`_0.08483,, 0)

            TCHZ_Split_Peak_Type(TCHZ09,-0.26097`_0.02239,TCHZ15,
0.01,TCHZ10,  0.00451`_0.00047,,  0,TCHZ11,  0.41253`_0.01931,,  0,TCHZ12,-
0.10456`_0.00755,TCHZ13,        0.04405`_0.00286,TCHZ14,-0.00209`_0.00023,,
0,TCHZ16, 0.00010`_0.00696,, 0)

            User_Defined_Dependence_Convolution(gauss_fwhm,     (2 Th)     ,
fwhm_middle, 1.13368`_0.08665 min 0.1 max 2)
```

Rietveld refinement of ex-situ data

Rietveld refinements of ex-situ Si-640d samples before and after milling mixed with LaB_6-660b internal standard, were performed with the software Topas V6. To allow for an easier comparison, the ex-situ scans collected with MoKα radiation were analysed up to 35º, thus including the first five reflections from Si as in the in-situ diffractograms. Structural parameters for Si and LaB_6 (B atomic *x* coordinate and individual thermal parameters for each atom) were refined. A spherical harmonics model was adopted for preferred orientation. A shifted Chebyshev function with six parameters was used to fit the background. The peak shape and the parameters describing the diffractometer geometry were modeled with a fundamental parameters approach using the LaB_6 NIST internal standard. The sample contribution to peak broadening was assumed to be Lorentzian and isotropic for both crystal size and microstrain related effects, which were estimated by incorporating the relative equations in the whole pattern refinement. The plots are shown in Figure R_{wp} = 2.54% and χ^2 = 1.32 pristine sample; and R_{wp} = 3.27% and χ^2 = 1.66 for the sample milled for 30 minutes. After 30 minutes of milling the crystal size of Si was found to be too large to be reliably estimated (larger than 1 μm), while ε_0 = 0.00065(3), in agreement with what we observe in situ.

Microstrain parameter definition

In general, the crystallinity of a sample is determined by its crystal size and strain. (Micro)strain ε_0 is the nonuniform variation in the unit cell and interplanar spacings *d* caused by local distortion of lattice planes. It is defined as $\Delta d/d$, and it is adimensional. The distortion is the direct consequence of defects such as vacancies, substitutions, or dislocations. The diffraction angle θ of radiation with wavelength λ depends on the interplanar spacing in agreement with Bragg's Law:

$$2\theta = 2arcsin\left(\frac{\lambda}{2d}\right)$$ Supplementary Equation 15

The more defects, the less constant is the value of *d*, and hence the broader will be the diffraction peaks (**Supplementary Figure 12**).

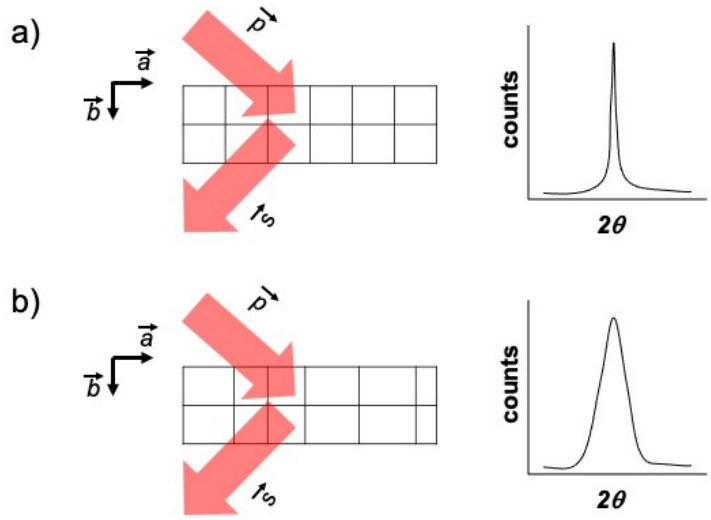

Figure SI 12| Schematic representation of the effect of non-uniform lattice distortion on the diffraction peak broadening: $\vec{a}$, $\vec{b}$ are the unit cell axes, represented by the rectangular grid; $\vec{p}$ and $\vec{s}$ represents the incident and diffracted radiation respectively. a) an undistorted lattice (left) yielding narrow diffraction peaks (right); b) non uniform distortion of the lattice along the $\vec{a}$ crystallographic direction, i.e. a distribution of the interplanar *d* spacings around an average $\vec{a}$ values (left), causing a broadening of the diffraction peaks.

Lattice parameters, scaling factors and CS parameters were refined individually for all scans. Each scan was normalized using the scale parameter of the empirical background at the end of the relative Rietveld refinement as a normalization factor. The sequential Rietveld refinement was then performed again as described in above. Size and strain for all four phases were refined with a Lorentzian and Gaussian function, respectively. A Lorentzian function was convoluted for each phase, with a single isotropic CS parameter related to Lorentzian peak width Γ_L as in the Scherrer Equation (**Supplementary Equations 1 and 2**) described in above. A Gaussian function was convoluted for each phase, with a single isotropic strain parameter e_0 related to Γ_G (the FWHM of a Gaussian curve) as in the following equation:

$$\varepsilon_0 = \frac{\Gamma_G(2\theta)}{4(tan\theta)}$$ Supplementary Equation 16

Thus, the strain contribution to peak broadening depends on the diffraction angle θ in a different way from CS, which makes deconvolution of sample CS and strain contributions possible.

Details of neat grinding reactions

Inorganic metathesis reaction by neat grinding

$$KI + CsCl \xrightarrow{NG} KCl + CsI$$

Scheme SI 1 | Chemical equation for reaction I via neat grinding

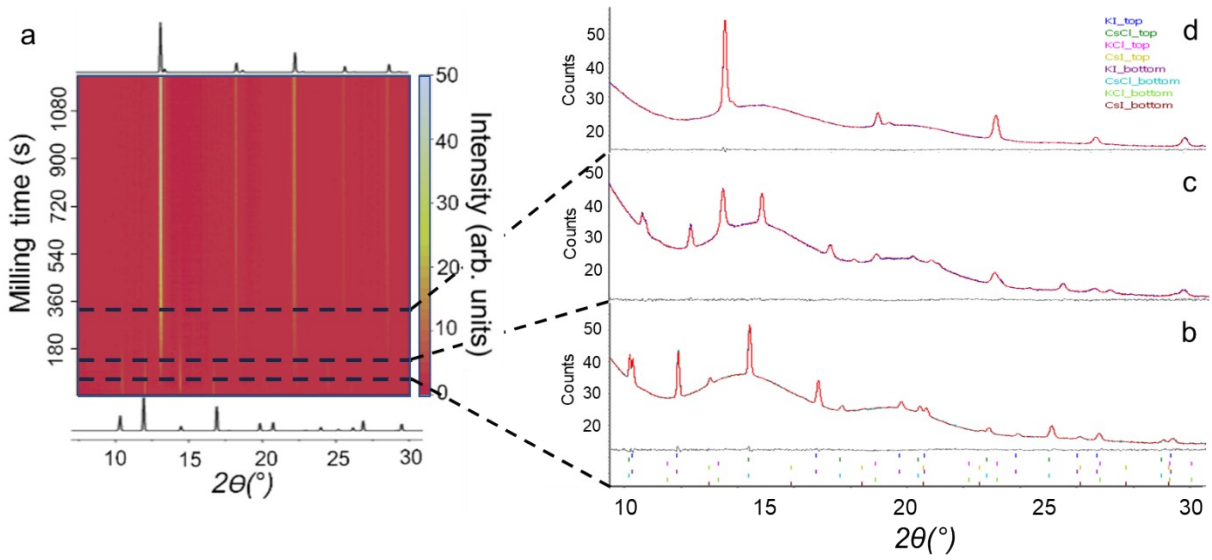

Figure SI 13| TRIS-XRPD for inorganic metathesis under ball mill neat grinding conditions with a loading of 70 mg. a. Heat maps (linear intensity, arb. units) of TRIS-XRPD with empirical background subtracted data alongside calculated 1D XRPD patterns for the reagents (KI + CsCl) and the final products (KCl + CsI). Representative Rietveld plots for the sequential refinement of the inorganic metathesis reaction: b) scan 010 representing the starting of the experiment; b) scan 028, halfway the experiment; c) scan 098, end of the experiment. Calculated profile (red line) against experimental data (black line) and difference pattern (grey line). Peak marks are shown for all phases twice, once for the inner scattering ring ("top" phases), and once for the outer scattering ring ("bottom" phases) – a legend with the corresponding colour for each phase is shown in the top right corner of (b).

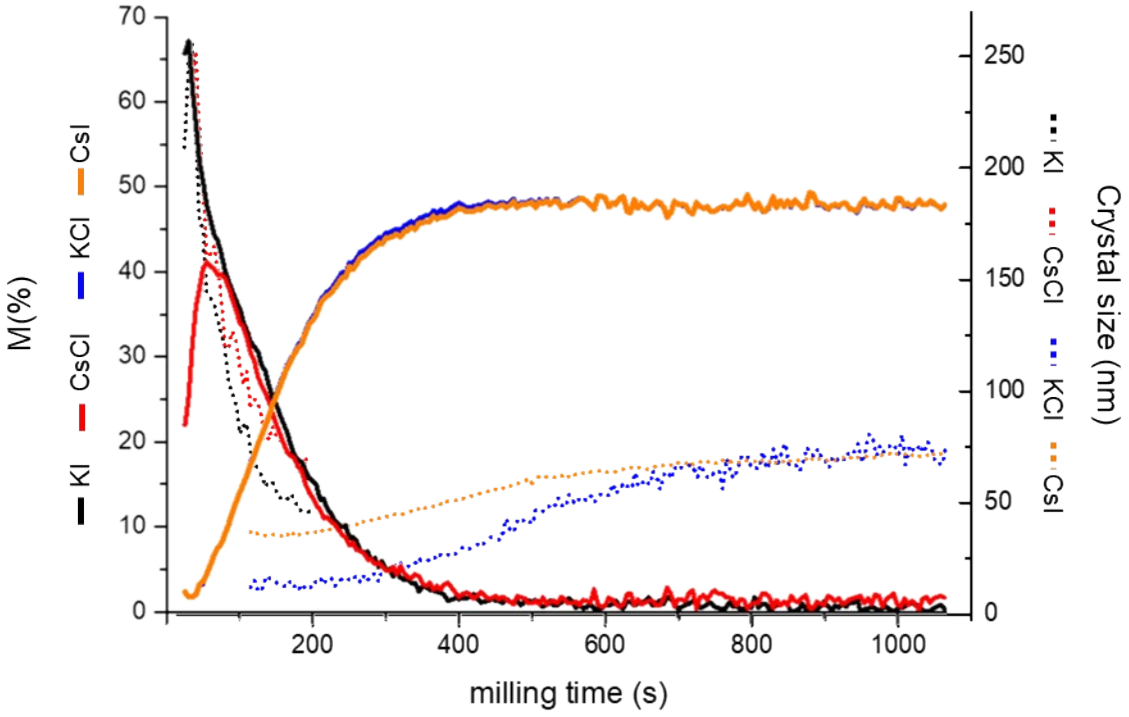

Figure SI 14| Quantitative phase analysis obtained by Rietveld refinement, showing the consumption of KI (solid black line) and CsCl (solid red line), with simultaneous formation of KCl (solid blue line) and CsI (solid orange line). ESD are omitted for the sake of clarity. Scherrer crystal size obtained for KI (dotted black line), CsCl (dotted red line), KCl (dotted blue line) and CsI (dotted orange line) for phases more abundant than 20 M% is superimposed. A legend with the corresponding colour for each phase is shown in the figure

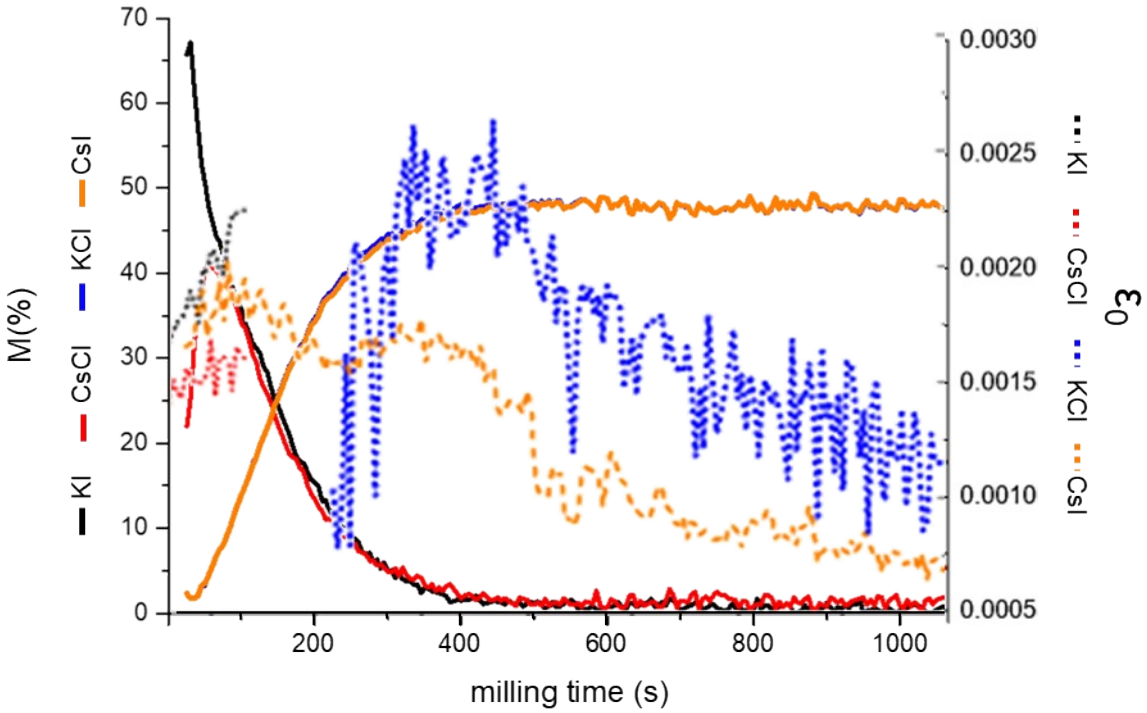

Figure SI 15| Quantitative phase analysis obtained by Rietveld refinement, showing the consumption of KI (solid black line) and CsCl (solid red line), with simultaneous formation of KCl (solid blue line) and CsI (solid orange line). ESD are omitted for the sake of clarity. Microstrian ε obtained for KI (dotted black line), CsCl (dotted red line), KCl (dotted blue line) and CsI (dotted orange line) for phases more abundant than 20 M% is superimposed. A legend with the corresponding colour for each phase is shown in the figure

Synthesis of Theophylline:Benzamide cocrystals

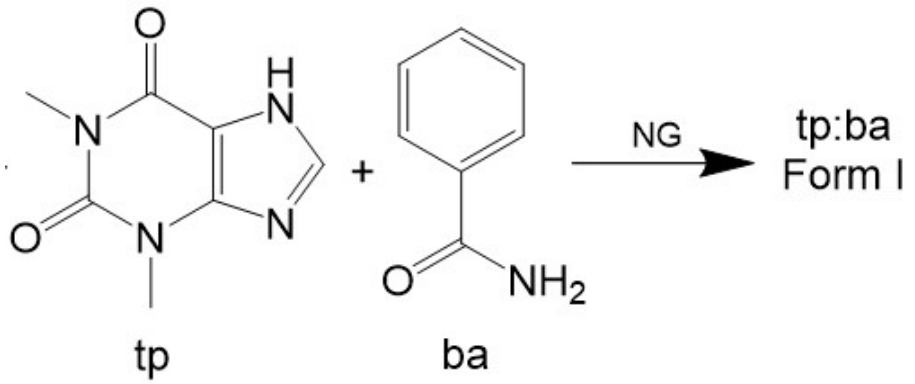

Scheme SI 2| Chemical equation for cocrystallizartion tp:ba 1:1. Form I is obtained via neat grinding.

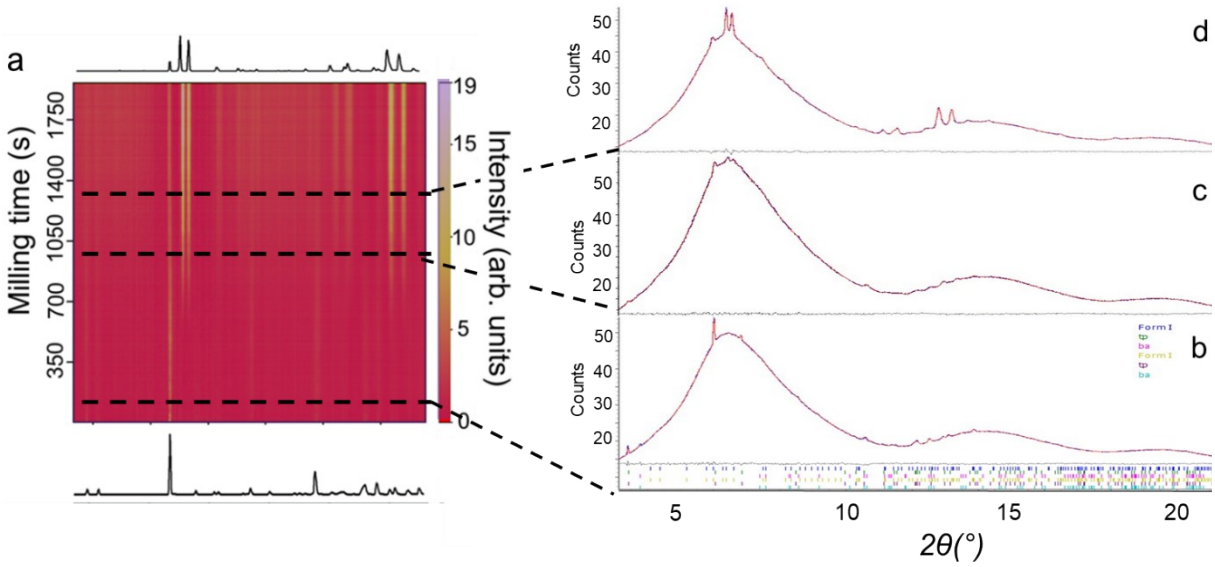

Figure SI 16| TRIS-XRPD for the cocrystallisation of the 1:1 cocrystal of theophylline (tp) and benzamide (ba) under ball mill neat grinding with 60 mg loading. a) Heat maps (linear intensity, arb. units) of TRIS-XRPD empirical background- subtracted data for the ball milling synthesis of tp:ba Form I alongside calculated 1D XRPD patterns for the coformer mixture (tp + ba) and the final products. Representative Rietveld plots for the sequential refinement of the organic cocrystallisation between theophylline (tp) and benzamide (ba) to produce Form I of the 1:1 tp:ba co-crystal: b) scan 005, start of the experiment; b) scan 148, halfway the experiment; c) scan 390, end of the experiment. calculated profile (red line) against experimental data (blue line) and difference pattern (grey line). Peak marks are shown for all phases twice, once for the inner scattering ring, and once for the outer scattering ring – a legend with the corresponding colour for each phase is shown in the top right corner of (b).

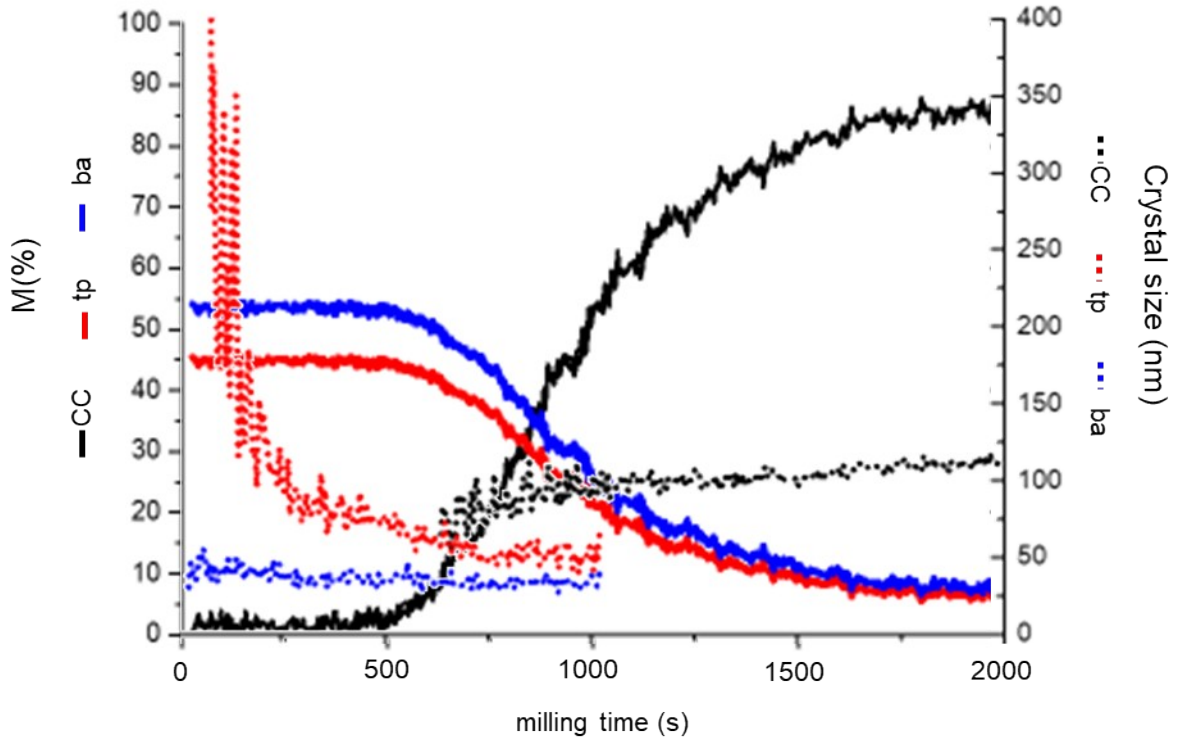

Figure SI 17| Quantitative phase analysis obtained by Rietveld refinement, showing the consumption of ba (solid blue line) and tp (solid red line), with simultaneous formation of cocrystal Form I (solid blacl line). ESD are omitted for the sake of clarity. Scherrer crystal size obtained for cocrystal Form I (dotted black line), tpl (dotted red line) and ba (dotted blue line) for phases more abundant than 20 M% is superimposed. A legend with the corresponding colour for each phase is shown in the figure.

TOPAS custom Macros

Sample displacement macro

The "*Peak_Split_2Th_displacement*" macro describes the peak splitting of the Bragg reflections of data collected in scanning mode in a physically meaningful way.

```
macro Peak_Split_2Th_displacement(beam_SD_V, beam_SD)
{
#m_argu beam_SD_V
If_Prm_Eqn_Rpt(beam_SD_V, beam_SD, min = Val-.1; max = Val+.1; del 0.001)
th2_offset = (Rad * ArcSin((CeV(beam_SD_V, beam_SD) * Sin(2 Th))/Rs));
}
```

Sample displacement macro with extra empirical correction

The "*Peak_Split_2Th_displacement_2D*" macro describes the peak splitting of the Bragg reflections of data collected with large flat area detectors in a physically meaningful way, including an extra empirical correction tunable for the detector dimensions.

```
macro Peak_Split_2Th_displacement_2D(beam_SD_V, beam_SD, m_V, m)
{
#m_argu beam_SD_V
If_Prm_Eqn_Rpt(beam_SD_V, beam_SD, min = Val-.1; max = Val+.1; del 0.001)
#m_argu m_V
If_Prm_Eqn_Rpt(m_V, m, min = -10; max = 10; del 0.001)
th2_offset = (Rad * ArcSin(((CeV(beam_SD_V, beam_SD) * Sin(2 Th))/Rs) + (CeV(m_V, m) * (Tan(2 Th))^2)));
}
```

TCHZ Peak profile for the split peak

The "TCHZ_Split_Peak_Type" macro models the asymmetric peak shape by splitting the TCHZ peak type into left and right sides.

```
macro TCHZ_Split_Peak_Type(u_Left, u_Leftv, v_Leftv, v_Left, w_Left, w_Leftv, z_Left, z_Leftv, x_Left,
  x_Leftv, y_Left, y_Leftv, u_Right, u_Rightv, v_Right, v_Rightv, w_Right, w_Rightv, z_Right, z_Rightv,
  x_Right, x_Rightv, y_Right, y_Rightv)
   {
      #m_argu u_Left
      #m_argu v_Left
      #m_argu w_Left
      #m_argu z_Left
      #m_argu x_Left
      #m_argu y_Left
      #m_argu u_Right
      #m_argu v_Right
      #m_argu w_Right
      #m_argu z_Right
      #m_argu x_Right
      #m_argu y_Right
      If_Prm_Eqn_Rpt(u_Left, u_Leftv, min = Max(-1, Val-.1); max = Min(2, Val+.1); del 1.0e-4)
      If_Prm_Eqn_Rpt(v_Left, v_Leftv, min = Max(-1, Val-.1); max = Min(2, Val+.1); del 1.0e-4)
      If_Prm_Eqn_Rpt(w_Left, w_Leftv, min = Max(-1, Val-.1); max = Min(2, Val+.1); del 1.0e-4)
      If_Prm_Eqn_Rpt(z_Left, z_Leftv, min = Max(-1, Val-.1); max = Min(2, Val+.1); del 1.0e-4)
      If_Prm_Eqn_Rpt(x_Left, x_Leftv, min = Max(0.0001, Val-.1); max = Min(2, Val+.1); del 1.0e-4 )
      If_Prm_Eqn_Rpt(y_Left, y_Leftv, min = Max(0.0001, Val-.1); max = Min(2, Val+.1); del 1.0e-4 )
      If_Prm_Eqn_Rpt(u_Right, u_Rightv, min = Max(-1, Val-.1); max = Min(2, Val+.1); del 1.0e-4)
      If_Prm_Eqn_Rpt(v_Right, v_Rightv, min = Max(-1, Val-.1); max = Min(2, Val+.1); del 1.0e-4)
      If_Prm_Eqn_Rpt(w_Right, w_Rightv, min = Max(-1, Val-.1); max = Min(2, Val+.1); del 1.0e-4)
      If_Prm_Eqn_Rpt(z_Right, z_Rightv, min = Max(-1, Val-.1); max = Min(2, Val+.1); del 1.0e-4)
      If_Prm_Eqn_Rpt(x_Right, x_Rightv, min = Max(0.0001, Val-.1); max = Min(2, Val+.1); del 1.0e-4 )
      If_Prm_Eqn_Rpt(y_Right, y_Rightv, min = Max(0.0001, Val-.1); max = Min(2, Val+.1); del 1.0e-4 )
      local #m_unique tch_p_l_Left = CeV(x_Left, x_Leftv) Tan(Th) + CeV(y_Left, y_Leftv) / Cos(Th);
      local #m_unique tch_p_g_Left = Sqrt( Abs( CeV(u_Left, u_Leftv) Tan(Th)^2 + CeV(v_Left, v_Leftv) Tan(Th)
  + CeV(w_Left, w_Leftv) + CeV(z_Left, z_Leftv) / Cos(Th)^2) );
      local #m_unique tch_p_Left =
         (
                    tch_p_g_Left^5 + 2.69269 tch_p_g_Left^4 tch_p_l_Left + 2.42843 tch_p_g_Left^3
  tch_p_l_Left^2 + 4.47163 tch_p_g_Left^2 tch_p_l_Left^3 + 0.07842 tch_p_g_Left   tch_p_l_Left^4 +
  tch_p_l_Left^5
        )^0.2;
      local #m_unique tch_q_Left = tch_p_l_Left / tch_p_Left;
      local #m_unique tch_p_l_Right = CeV(x_Right, x_Rightv) Tan(Th) + CeV(y_Right, y_Rightv) / Cos(Th);
      local #m_unique tch_p_g_Right = Sqrt( Abs( CeV(u_Right, u_Rightv) Tan(Th)^2 + CeV(v_Right, v_Rightv)
  Tan(Th) + CeV(w_Right, w_Rightv) + CeV(z_Right, z_Rightv) / Cos(Th)^2) );
      local #m_unique tch_p_Right =
```

```
       (
                  tch_p_g_Right^5 + 2.69269 tch_p_g_Right^4 tch_p_l_Right + 2.42843 tch_p_g_Right^3
tch_p_l_Right^2 + 4.47163 tch_p_g_Right^2 tch_p_l_Right^3 + 0.07842 tch_p_g_Right tch_p_l_Right^4 +
                           tch_p_l_Right^5
       )^0.2;
     local #m_unique tch_q_Right = tch_p_l_Right / tch_p_Right;
     peak_type spv
        spv_l1 = 1.36603 tch_q_Left - 0.47719 tch_q_Left^2 + 0.1116 tch_q_Left^3;
        spv_h1 = tch_p_Left;
        spv_l2 = 1.36603 tch_q_Right - 0.47719 tch_q_Right^2 + 0.1116 tch_q_Right^3;
          spv_h2 = tch_p_Right;
```

Refinement of the peak split

The "*Triplet_Split_Peak_2D*" macro separates the right, middle and left components of each Bragg reflection. The left and right components are described by an independently refinable sample displacement parameter and by the TCHZ split peak type function. The middle contribution is described by a Gaussian function convolution. A refinable scale factor is also added to account for the different intensity of each peak component. This macro is particularly indicated for data collected in scanning mode.

```
macro Triplet_Split_Peak( sL, sL_v, oL, oL_v,    sM, sM_v, oM, oM_v,    sR, sR_v, oR, oR_v)
{
        'Initialize variables
                #m_argu sL 'scale of left peak
                #m_argu oL 'offset of left peak
                #m_argu sM 'scale of middle peak
                #m_argu oM 'offset of middle peak
                #m_argu sR 'scale of right peak
                #m_argu oR 'offset of right peak

                If_Prm_Eqn_Rpt(sL, sL_v, min 0, )
                If_Prm_Eqn_Rpt(oL, oL_v, min -10 max 10,)
                If_Prm_Eqn_Rpt(sM, sM_v,min 0, )
                If_Prm_Eqn_Rpt(oM, oM_v,min -10 max 10,)
                If_Prm_Eqn_Rpt(sR, sR_v,min 0, )
                If_Prm_Eqn_Rpt(oR, oR_v,min -10 max 10,)

'left peak
      str
        TCHZ_Split_Peak_Type( @ ,=TCHZ01_L; ,, 0.01 , @  ,=TCHZ03_L; ,, 0, @ , =TCHZ04_L; ,, 0,  @
,=TCHZ05_L; ,  @ , =TCHZ06_L; , @ ,=TCHZ07_L; ,, 0 , @ , =TCHZ08_L; ,, 0)
        Peak_Split_2Th_displacement( @  ,= CeV(oL, oL_v); )
        scale  = CeV(sL, sL_v)/1e10;
'middle peak
      str
        User_Defined_Dependence_Convolution(gauss_fwhm,   (2 Th)   , @ , =GaussFWHM_M; min 0.1 max 1)
        Peak_Split_2Th_displacement( @  ,  = CeV(oM, oM_v);)
        scale  = CeV(sM, sM_v)/1e10;
'right peak
      str
        TCHZ_Split_Peak_Type( @ ,=TCHZ01_R; ,, 0.01 ,  @ ,=TCHZ03_R; ,, 0, @ , =TCHZ04_R; ,, 0,  @
,=TCHZ05_R; ,  @ , =TCHZ06_R; , @  ,=TCHZ07_R; ,, 0 ,@  , =TCHZ08_R; ,, 0)
        Peak_Split_2Th_displacement( @ ,= CeV(oR, oR_v);)
        scale  = CeV(sR, sR_v)/1e10;
}
```

The "*Triplet_Split_Peak_2D*" macro separates the right, middle and left components of each Bragg reflection. The left and right components are described by an independently refinable sample displacement parameter and by the TCHZ split peak type function. The middle contribution is described by a Gaussian function convolution. A refinable scale factor is also added to account for the different intensity of each peak component. A refinable correction for the use of large flat area detectors is considered.

```
macro Triplet_Split_Peak_2D( sL, sL_v, oL, oL_v, sM, sM_v, oM, oM_v, sR, sR_v, oR, oR_v, FDcorr, FDcorr_v)
{
        'Initialize variables
                #m_argu sL 'scale of left peak
                #m_argu oL 'offset of left peak
                #m_argu sM 'scale of middle peak
                #m_argu oM 'offset of middle peak
                #m_argu sR 'scale of right peak
                #m_argu oR 'offset of right peak
                #m_argu FDcorr 'correction for flat detector dimension
```

```
                If_Prm_Eqn_Rpt(sL, sL_v, min 0, )
                If_Prm_Eqn_Rpt(oL, oL_v, min -10 max 10,)
                If_Prm_Eqn_Rpt(sM, sM_v,min 0, )
                If_Prm_Eqn_Rpt(oM, oM_v,min -10 max 10,)
                If_Prm_Eqn_Rpt(sR, sR_v,min 0, )
                If_Prm_Eqn_Rpt(oR, oR_v,min -10 max 10,)
                If_Prm_Eqn_Rpt(FDcorr, FDcorr_v, min -10 max 10,)

'left peak
      str
        TCHZ_Split_Peak_Type( @ ,=TCHZ01_L; ,, 0.01 , @  ,=TCHZ03_L; ,, 0, @ , =TCHZ04_L; ,, 0,  @
,=TCHZ05_L; ,  @ , =TCHZ06_L; , @ ,=TCHZ07_L; ,, 0 , @ , =TCHZ08_L; ,, 0)
        Peak_Split_2Th_displacement_2D( @  ,= CeV(oL, oL_v);, @ ,= CeV(FDcorr, FDcorr_v);)
        scale  = CeV(sL, sL_v)/1e10;
'middle peak
      str
        User_Defined_Dependence_Convolution(gauss_fwhm,   (2 Th)   , @ , =GaussFWHM_M; min 0.1 max 1)
        Peak_Split_2Th_displacement( @  ,= CeV(oM, oM_v); )
        scale  = CeV(sM, sM_v)/1e10;
'right peak
      str
        TCHZ_Split_Peak_Type( @ ,=TCHZ01_R; ,, 0.01 ,  @ ,=TCHZ03_R; ,, 0, @ , =TCHZ04_R; ,, 0,  @
,=TCHZ05_R; ,  @ , =TCHZ06_R; , @  ,=TCHZ07_R; ,, 0 ,@  , =TCHZ08_R; ,, 0)
        Peak_Split_2Th_displacement_2D( @  ,= CeV(oR, oR_v);, @ ,= CeV(FDcorr, FDcorr_v);)
        scale  = CeV(sR, sR_v)/1e10;
}
```

The "*Doublet_Split_Peak*" macro separates the right and left components of each Bragg reflection. The left and right components are described by an independently refinable sample displacement parameter and by the TCHZ split peak type function. A refinable scale factor is also added to account for the different intensity of each peak component. This macro is particularly indicated for data collected in scanning mode.

```
macro Doublet_Split_Peak( sL, sL_v, oL, oL_v, sR, sR_v, oR, oR_v)
{
        'Initialize variables
                #m_argu sL 'scale of left peak
                #m_argu oL 'offset of left peak
                #m_argu sR 'scale of right peak
                #m_argu oR 'offset of right peak

                If_Prm_Eqn_Rpt(sL, sL_v, min 0, )
                If_Prm_Eqn_Rpt(oL, oL_v, min -10 max 10,)
                If_Prm_Eqn_Rpt(sR, sR_v,min 0, )
                If_Prm_Eqn_Rpt(oR, oR_v,min -10 max 10,)

'left peak
      str
        TCHZ_Split_Peak_Type( @ ,=TCHZ01_L; ,, 0.01 , @  ,=TCHZ03_L; ,, 0, @ , =TCHZ04_L; ,, 0,  @
,=TCHZ05_L; ,  @ , =TCHZ06_L; , @ ,=TCHZ07_L; ,, 0 , @ , =TCHZ08_L; ,, 0)
        Peak_Split_2Th_displacement( @  ,= CeV(oL, oL_v); )
        scale  = CeV(sL, sL_v)/1e10;
'right peak
      str
        TCHZ_Split_Peak_Type( @ ,=TCHZ01_R; ,, 0.01 ,  @ ,=TCHZ03_R; ,, 0, @ , =TCHZ04_R; ,, 0,  @
,=TCHZ05_R; ,  @ , =TCHZ06_R; , @  ,=TCHZ07_R; ,, 0 ,@  , =TCHZ08_R; ,, 0)
        Peak_Split_2Th_displacement( @ ,= CeV(oR, oR_v);)
        scale  = CeV(sR, sR_v)/1e10;
}
```

The "*Doublet_Split_Peak_2D*" macro separates the right and left components of each Bragg reflection. The left and right components are described by an independently refinable sample displacement parameter and by the TCHZ split peak type function. A refinable scale factor is also added to account for the different intensity of each peak component. A refinable correction for the use of large flat area detectors is considered.

```
macro Doublet_Split_Peak_2D( sL, sL_v, oL, oL_v, sR, sR_v, oR, oR_v, FDcorr, FDcorr_v)
{
        'Initialize variables
                #m_argu sL 'scale of left peak
                #m_argu oL 'offset of left peak
                #m_argu sR 'scale of right peak
                #m_argu oR 'offset of right peak
```

```
                If_Prm_Eqn_Rpt(sL, sL_v, min 0, )
                If_Prm_Eqn_Rpt(oL, oL_v, min -10 max 10,)
                If_Prm_Eqn_Rpt(sR, sR_v,min 0, )
                If_Prm_Eqn_Rpt(oR, oR_v,min -10 max 10,)
                If_Prm_Eqn_Rpt(FDcorr, FDcorr_v, min -10 max 10,)

'left peak
      str
        TCHZ_Split_Peak_Type( @ ,=TCHZ01_L; ,, 0.01 , @  ,=TCHZ03_L; ,, 0, @ , =TCHZ04_L; ,, 0,  @
,=TCHZ05_L; ,  @ , =TCHZ06_L; , @ ,=TCHZ07_L; ,, 0 , @ , =TCHZ08_L; ,, 0)
        Peak_Split_2Th_displacement_2D( @  ,= CeV(oL, oL_v);, @ ,= CeV(FDcorr, FDcorr_v);)
        scale  = CeV(sL, sL_v)/1e10;
'right peak
      str
        TCHZ_Split_Peak_Type( @ ,=TCHZ01_R; ,, 0.01 ,  @ ,=TCHZ03_R; ,, 0, @ , =TCHZ04_R; ,, 0,  @
,=TCHZ05_R; ,  @ , =TCHZ06_R; , @  ,=TCHZ07_R; ,, 0 ,@  , =TCHZ08_R; ,, 0)
        Peak_Split_2Th_displacement_2D( @  ,= CeV(oR, oR_v);, @ ,= CeV(FDcorr, FDcorr_v);)
        scale  = CeV(sR, sR_v)/1e10;
}
```